Laser-Driven Magnetic Reconnection: Near- and Far-field Observations of Plasma Outflow

Morita, T.
Faculty of Engineering Sciences, Kyushu University

Takezaki, T.
Faculty of Engineering, University of Toyama

Isayama, S.
Faculty of Engineering Sciences, Kyushu University

Ogawa, T.
Interdisciplinary Graduate School of Engineering Sciences, Kyushu University

他

https://hdl.handle.net/2324/7440041

出版情報：JJAP Conference Proceedings, pp.011015-, 2026. 応用物理学会
バージョン：

Laser-Driven Magnetic Reconnection: Near- and Far-field Observations of Plasma Outflow

T. Morita[1*], T. Takezaki[2], S. Isayama[1], T. Ogawa[3], K. Koba[3], M. Edamoto[4], K. Iida[5], F. Ishizaki[2], A. Kashima[6], H. Kawakatsu[6], H. Kondo[6], S. Kurimaru[3], S. Matsukiyo[1], K. Nakahara[3], K. Okabe[6], K. Sakai[7], T. Sano[8], R. Shiiba[3], S. J. Tanaka[6], K. Tomita[9], Y. Toyoda[10], S. Yakura[6], R. Yamazaki[6], and Y. Sakawa[8]

[1]Faculty of Engineering Sciences, Kyushu University, 6-1 Kasuga-Koen, Kasuga, Fukuoka 816-8580, Japan.
[2]Faculty of Engineering, University of Toyama, Gofuku 3190, Toyama-shi, Toyama 930-8555, Japan.
[3]Interdisciplinary Graduate School of Engineering Sciences, Kyushu University, 6-1, Kasuga-Koen, Kasuga, Fukuoka 816-8580, Japan.
[4]Faculty of Science and Technology, Seikei University, Kichijoji, Musashino, Tokyo 180-8633, Japan
[5]Graduate School of Engineering, The University of Osaka, 2-1 Yamadaoka, Suita, Osaka 565-0871, Japan.
[6]Department of Physical Sciences, Aoyama Gakuin University, 5-10-1 Fuchinobe, Sagamihara, Kanagawa 252-5258, Japan.
[7]National Institute for Fusion Science, 322-6 Oroshi-cho, Toki, Gifu 509-5292, Japan.
[8]Institute of Laser Engineering, The University of Osaka, 2-6 Yamadaoka, Suita, Osaka 565-0871, Japan.
[9]Faculty of Engineering, Hokkaido University, Kita 13, Nishi 8, Kita-ku, Sapporo, Hokkaido 060-8628, Japan.
[10]Graduate School of Science, The University of Osaka, 2-1 Yamadaoka, Suita, Osaka 565-0871, Japan.

* E-mail : morita@aees.kyushu-u.ac.jp

Abstract. Magnetic reconnection, a fundamental process driving energy release across laboratory, space, and astrophysical plasmas, efficiently converts magnetic field energy into plasma kinetic and thermal energy. Here, we present the simultaneous, direct observation of plasma outflow acceleration across different spatial scales in laser-produced plasmas: the near-field (local acceleration) and the far-field (the resulting plasma jet). Local plasma flow near the X-point is measured using the Doppler shift of Thomson scattering spectra. The resultant high-speed plasma jet emanating from the reconnection region is subsequently detected by an ion collector with a Faraday cup. The near- and far-field velocity measurements exhibit a similar tendency across three different initial plasma conditions. This simultaneous diagnostic approach provides a powerful tool for the detailed experimental investigation and validation of magnetic reconnection physics.

1. Introduction

Magnetic reconnection [1, 2] is ubiquitous in various plasma environments, such as astrophysical, space, and laboratory plasmas, where it converts magnetic field energy into plasma kinetic and thermal energy. However, several unsolved problems remain regarding reconnection physics, including the reconnection rate, the partition of energy conversion between ions and electrons (and between thermal and kinetic energies), and non-thermal particle acceleration.

Recently, magnetic reconnection has been investigated using high-power lasers. Laser-produced plasma is readily magnetized due to the Biermann battery effect [3], making it possible to form an anti-parallel magnetic field configuration. The magnetic field structure during the reconnection process has been visualized by proton radiography, while plasma parameters have been inferred using laser Thomson scattering [4]. Proton radiography reveals the magnetic field structure, including current-sheet formation and the time-evolution of the reconnection field [5–7]. Laser Thomson scattering spectra, on the other hand, reveal plasma parameters before and after the reconnection, such as electron and ion acceleration, and current-sheet formation [8–11]. However, reconnection involves kinetic effects on the electron scale (where ions are unmagnetized) and resultant field topology changes on the global magnetohydrodynamic (MHD) scale. Consequently, it can be challenging to identify reconnection properties solely from local measurements or the magnetic field structure, making it difficult to fully understand the entire process, including the determination of the reconnection rate and the energy conversion process.

To address this challenge, we perform simultaneous near- and far-field measurements of a plasma jet accelerated via magnetic reconnection using a high-power laser system. The acceleration of plasma near the reconnection site is investigated using the laser Thomson scattering method. The plasma is then extracted from the reconnection region as an outflow plasma jet, which is measured with an ion collector near the chamber wall, far from the reconnection site. The plasma plumes decelerate during their interaction, but can be subsequently accelerated due to magnetic reconnection. This plasma jet arrives at the detector as a slower ion component. This simultaneous near- and far-field measurement approach offers the potential to reveal the dynamics of plasma outflow jet formation during the reconnection process.

2. Experimental method

The experiment was performed using the high-power Gekko XII laser system at Osaka University. As shown in Fig. 1(a), two carbon foils were irradiated by two high-energy laser beams (energy of ∼700 J per beam in 1.3 ns at a wavelength of 1053 nm) to generate two plasma plumes. Generally, the ablation plasma is magnetized via the Biermann battery effect, which is attributed to anisotropic, large gradients of electron temperature and density [3]. The two laser spots were separated by 1, 1.5, or 2 mm

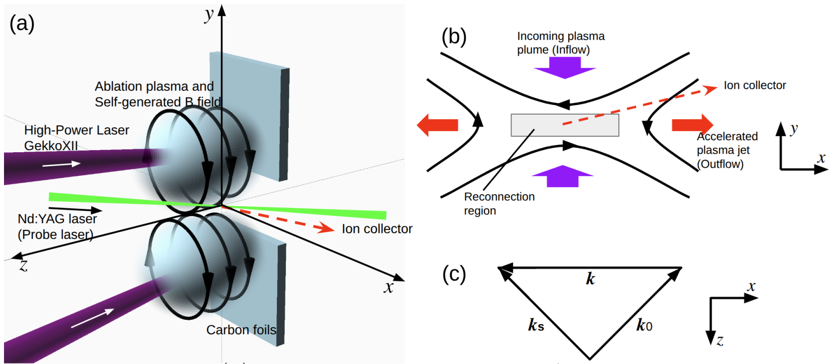

Figure 1. (a) Experimental layout of the interaction between two plasma plumes. Another low-energy laser (probe laser) is incident for Thomson scattering measurement. (b) Magnetic field structure in the mid-plane. (c) The vector relation of the wavenumber of incident and scattered light, and of the ion-acoustic wave excited in the plasma.

in different laser shots to investigate the dependence on initial plasma parameters. An anti-parallel magnetic field structure was formed between the two plumes, as illustrated in Fig. 1(b). The plasmas, carrying anti-directional magnetic fields, approach from the top and bottom. As the magnetic fields in the upper and lower regions reconnect, the reconnected field expands sideways, accelerating the plasma as an outflow.

The reconnection region in the mid-plane is diagnosed using the laser Thomson scattering method. This utilized a separate probe laser (Nd:YAG) with a wavelength of 532 nm, focused at the center of the two laser spots to a focal diameter of approximately 100 μm. Figure 1(c) illustrates the vector relation of the wavenumbers: $\boldsymbol{k}_\mathrm{i}$ for the incident probe laser, $\boldsymbol{k}_\mathrm{s}$ for the scattered light, and $\boldsymbol{k}$ for the ion-acoustic wave excited in the plasma.

The outflow emanating from the reconnection region was detected using an ion collector positioned near the vacuum chamber wall. It was located 647 mm from the center, a distance significantly larger than both the reconnection region ($\sim$100 μm) and the typical plasma scale (a few mm). As detailed in Fig. 1(d), the ion collector consists of a pinhole (2 mm diameter) serving as the plasma entrance and a Faraday cup to collect the ions. The cup was negatively biased (specifically, -100 V) to repel the electrons. The Faraday cup was connected to the ground via a 50 Ω resistor and a 50 Ω coaxial cable, and the voltage across the resistor was measured with an oscilloscope.

3. Results and discussion

Figures 2(a), 2(d), and 2(g) show the spectra of Thomson scattered light along the probe laser axis for laser-spot separations of 1, 1.5, and 2 mm, recorded at times of 6, 12, and 15 ns, respectively. The horizontal axis displays the wavelength and the vertical axis, p, shows the position along the probe laser. The scattered light at the probe wavelength, $\lambda = \lambda_0 = 532$ nm, is blocked by a notch filter in the spectrometer to avoid strong stray light. The two visible peaks represent the ion-acoustic resonance. The deviation of the center of these two peaks from λ_0 indicates a Doppler shift caused by the plasma

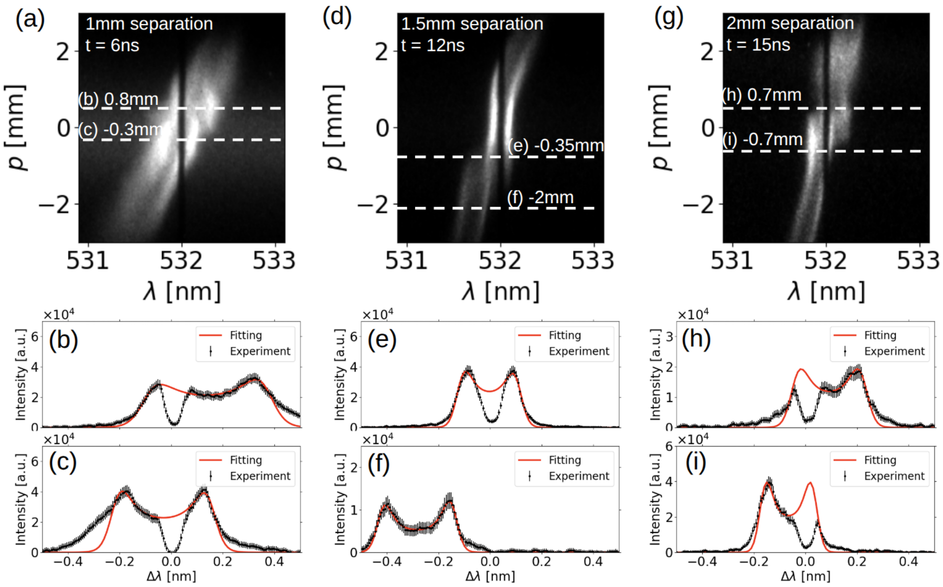

Figure 2. Ion-acoustic resonance measured by using Laser Thomson scattering method with different laser-spot separations of (a) 1 mm, (d) 1.5 mm, and (g) 2 mm. The vertical axis shows the distance along the probe laser. The spectra for two different positions before and after large Doppler shift are shown for (b,c) 1 mm, (e,f) 1.5 mm, and (h,i) 2 mm beam separations.

flow velocity. A sudden change in the Doppler shift is observed at certain positions, specifically at 0 mm in Fig. 2(a), 1 mm in Fig. 2(d), and 0 mm in Fig. 2(g). Line-out spectra detailing the regions before and after this velocity change are presented for the three different laser spot separations in Figs. 2(b) and 2(c); Figs. 2(e) and 2(f); and Figs. 2(h) and 2(i). In these line-out plots, the horizontal axis represents the wavelength difference, $\Delta\lambda = \lambda - \lambda_0$.

The red lines represent the fitted spectra using the theoretical spectral density function: $S(k,\omega) = 2\pi/k\left[\left|1-\chi_{\rm e}/\epsilon\right|^2 f_{\rm e}(\omega/k) + Z_{\rm i}\left|\chi_{\rm e}/\epsilon\right|^2 f_{\rm i}(\omega/k)\right]$ [4], where the subscripts e and i denote electron and ion, respectively. Here, $\boldsymbol{k} = \boldsymbol{k}_{\rm s} - \boldsymbol{k}_0$ and $\omega = \omega_{\rm s} - \omega_0$ are the wavenumber and frequency of the plasma wave, $\boldsymbol{k}_0$ and $\boldsymbol{k}_{\rm s}$ are the wavenumbers of the incident and scattered light, ω_0 and $\omega_{\rm s}$ are their corresponding frequencies, and ϵ and $\chi_{\rm e}$ are the longitudinal dielectric function and electron susceptibility, respectively. The flow velocities estimated from the fitting are $v_x = -56.7 \pm 3.8$ and 12.4 ± 1.5 km/s at $p = 0.8$ and -0.3 mm for Figs. 2(b) and 2(c), respectively, 1.4 ± 0.7 and 113 ± 3 km/s at $p = -0.35$ and -2 mm for Figs. 2(e) and 2(f), respectively, and -36.7 ± 0.9 and 26.2 ± 1.0 km/s at $p = 0.7$ and -0.7 mm for Figs. 2(h) and 2(i), respectively. The velocity jump observed between the interaction region and the outflow region is interpreted as the acceleration driven by magnetic reconnection as previously discussed in similar experimental configuration [10]. The calculated velocity increases and corresponding kinetic energy gains are: 69 ± 4 km/s (298 ± 35 eV), 112 ± 3 km/s (785 ± 42 eV), and 63 ± 1 km/s (249 ± 8 eV) for the 1, 1.5, and 2 mm spot separations, respectively

Figures 3(a)–3(c) show the ion current densities detected by the Faraday cup (Fig.

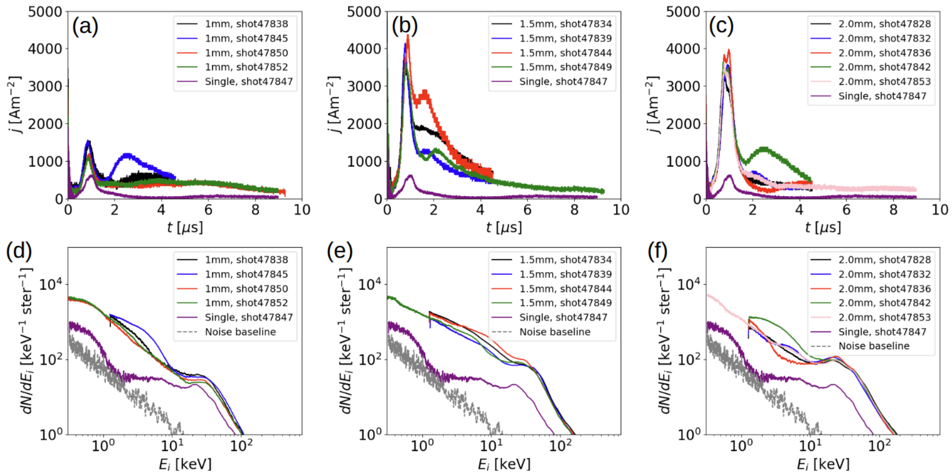

Figure 3. Ion current density measured with an ion collector for (a) 1 mm, (b) 1.5 mm, and (c) 2 mm beam spot separations. Ion velocity distribution estimated for each spot separations are shown for (d)–(f).

1(d)) for the 1, 1.5, and 2 mm spot separations. The purple solid line represents the current density from a single-laser beam ablation, while the other colored solid lines show the results from two-beam shots under the same target and laser conditions. Two distinct ion components are visible: an early component arriving around ~ 1 μs and a later component arriving around $\sim$2–4 μs. The energy distribution, dN/dE_i, is calculated for the three conditions and presented in Figs. 3(d)–3(f). The number of ions per solid angle, N, is determined from the current density, j, as $dN/dt = j/(Z_\mathrm{i} e \Delta\Omega)$, where e is the elementary charge, $Z_\mathrm{i} = 6$ is assumed for fully ionized carbon ions, and $\Delta\Omega$ is the solid angle of the entrance pinhole. The ion kinetic energy is $E_\mathrm{i} = m_\mathrm{i} v_\mathrm{i}^2/2$, derived from the time-of-flight velocity $v_\mathrm{i} = L/t$, where $L = 647$ mm is the distance to the Faraday cup.

When the two plasma plumes interact, the magnetic field is compressed, leading to a deceleration of the plume expansion. Following reconnection, the plasma is accelerated by the reconnected field in the $\pm x$-directions. This suggests that the outflow, despite being accelerated, may arrive at the detector later in time. The gray dashed line indicates the baseline noise. Comparing the noise and single-beam signals reveals distinct low-energy and high-energy components. The high-energy component ($t < 1.7$ μs in Figs. 3(a)–3(c), or $E_\mathrm{i} > 9$ keV in Figs. 3(d)–3(f)) is present in both single- and double-beam shots, confirming it is the high-speed expanding laser-produced plasma. The low-energy component ($t > 5$ μs or $E_\mathrm{i} < 1$ keV) is significantly slower and is interpreted as plasma originating from solid materials ablated by strong plasma radiation or collisions with the high-energy plasma.

Crucially, for the 1.5 mm separation (Fig. 3(b)), a third ion component emerges around ~ 2 μs, corresponding to an energy of ~ 7 keV (within the 1–9 keV range) in Fig. 3(e). This component is observed only in the double-beam irradiation shots, strongly linking it to the interaction between the two plasma plumes. Furthermore, this middle-energy component for the 1.5 mm separation is faster than the corresponding components for the 1 mm and 2 mm separations (observed at $t \sim 2.5$ μs in Figs. 3(a) and 3(c)). This suggests more efficient acceleration occurs at the 1.5 mm separation. This finding is consistent with the Thomson scattering data, which showed the largest Doppler effect and a plasma energization of 785 eV for the 1.5 mm separation, compared to smaller energizations of 298 eV and 249 eV for the 1 mm and 2 mm separations, respectively.

In summary, we conducted a laboratory experiment to investigate laser-driven magnetic reconnection using self-generated magnetic fields. Plasma acceleration via magnetic reconnection was studied using two complementary diagnostics: laser Thomson scattering for the near-field (local acceleration) and an ion collector for the far-field outflow measurement. The Thomson scattering spectra confirm plasma acceleration within the reconnection region, while the ion collector detects the resulting ion energy distribution far downstream. Both diagnostics demonstrate plasma acceleration, with the outflow being most efficiently accelerated at the 1.5 mm beam separation. While the precise reason for this optimal condition is currently unclear, acceleration is known to depend on initial plasma parameters and magnetic field strength. Future experiments will further investigate this dependence using multi-point and multi-directional laser Thomson scattering, along with multiple ion collectors positioned at various angles.

Acknowledgments

The authors would like to acknowledge the dedicated technical support of the staff at the Gekko-XII facility for the laser operation, target fabrication, and plasma diagnostics. We would also like to thank N. Ozaki for the target alignment in the experiment, and N. Yamamoto for helpful comments and valuable discussions. This research was partially supported by JSPS KAKENHI Grant Nos. JP24K00605, JP23H04864, and JP22H00119, and by the joint research project of Institute of Laser Engineering, Osaka University.

Reference

[1] E. G. Zweibel *et al.*, *Annu. Rev. Astron. Astrophys.* **47** 291–332 (2009)
[2] M. Yamada *et al. Rev. Mod. Phys.* **82** 603–664 (2010)
[3] J. A. Stamper *et al. Laser Part. Beams* **9** 841–862 (1991)
[4] J. Sheffield *et al. Plasma Scattering of Electromagnetic Radiation: Theory and Measurement Techniques* (Academic Press Inc)
[5] Z. Zhao *et al. Communications Physics* **5** 1–11 (2022)
[6] J. Zhong *et al.*, *High Power Laser Science and Engineering* **6** e48 (2018)
[7] M. J. Rosenberg *et al.*, *Phys. Rev. Lett.* **114** 205004 (2015)
[8] T. Morita *et al.*, *High Energy Density Phys.* **36** 100754 (2020)
[9] K. Sakai *et al.*, *Sci. Rep.* **12** 10921 (2022)
[10] T. Morita *et al.*, *Phys. Rev. E* **106** 055207 (2022)
[11] S. Zhang *et al.*, *Nat. Phys.* **19** 909–916 (2023)